IEEE Access
Multidisciplinary ⋮ Rapid Review ⋮ Open Access Journal

Received August 11, 2020, accepted August 27, 2020, date of publication September 2, 2020, date of current version September 17, 2020.

Digital Object Identifier 10.1109/ACCESS.2020.3021206

Research on the Model and the Location Method of Ship Shaft-Rate Magnetic Field Based on Rotating Magnetic Dipole

PENGFEI LIN, NING ZHANG, MING CHANG, AND LEI XU

College of Weaponry Engineering, Naval University of Engineering, Wuhan 430033, China

Corresponding author: Ning Zhang (18602710800@163.com)

This work was supported in part by the Science and Technology Commission of the CMC Foundation Strengthening Fund under Grant 2019-JCJQ-JJ-055.

ABSTRACT In this paper, the ship's rotating propeller is a considered as rotating magnetic dipole. The shaft-rate magnetic field is modeled, and an inversion calculation is utilized to realize the magnetic target localization. The low frequency of the shaft-rate magnetic field provides long propagation distance, high stability, and low interference by sea conditions and other noises. The magnetic field signal has an important role in target and location detection. In the developed model, the magnetic moment of the rotating magnetic dipole is decomposed into three orthogonal magnetic moments indicated by m_p, m_f and m_l. The mentioned moments can be obtained through a three-component integration of the measured magnetic field of the rotating dipole at a point. The relation between the eigenvectors of these orthogonal magnetic moments and the coordinates of the observation position is employed to obtain the coordinates and the magnetic target position. In the simulation, the relative and absolute errors of the location method are analyzed, while the measurement noise confines the positioning distance. Finally, the rotating magnetic field of 80 points is measured, and the feasibility of the rotating magnetic model is verified. Besides, the relative mean error of 80 points is equal to 3.7%, demonstrating the feasibility of the location method. However, due to some experiment limitations, including the measurement distance, measurement error, and the experimental equipment sensitivity, the maximum relative error is obtained as 7.4% which is higher than its theoretical value.

INDEX TERMS Location method, magnetic field distribution, orthogonal magnetic moments, rotating magnetic dipole.

I. INTRODUCTION

A variety of works has been devoted to the detection and location of underwater ship targets in several countries [1], [2]. The ship's magnetic field has a vital role in magnetic target detection in water. Various methods have been proposed for the ship's magnetic field detection and location. Jia et.al employed the Euler localization method of magnetic gradient tensor information to develop an improved Euler method in the form of an over-determined equation. Accordingly, an effective solution for the positioning failure problem has been presented, and the stability and effectiveness of the location method have been improved [3]. Yin, and Zhang proposed an explicit localization relation for magnetic dipole localization by measuring its magnetic field vector and magnetic gradient tensor, which provides the correct dipole position regardless of the singularity of magnetic gradient tensor matrix [4]. Song et.al have modeled the cylindrical magnet to construct a magnetic localization and orientation system. Moreover, they have built a sensor array for magnetic positioning. Although the feasibility of their proposed system was demonstrated through their extensive simulations and experiments [5], all these studies focus on the static magnetic field. Since the static magnetic field of ships propagates in a short distance and is significantly affected by the geomagnetic field, positioning distance of the above methods is short, and they also require more magnetic sensors [6], [7]. In contrast, the ship shaft-rate magnetic field has an extremely low frequency (ELF) magnetic field with a long propagation distance and little interference from the geomagnetic field [8].

The associate editor coordinating the review of this manuscript and approving it for publication was Mehmet Alper Uslu.

The ELF magnetic field of a ship mainly consists of the following two parts: a) A magnetic field with a particular frequency produced by the periodic modulation of corrosion or anti-corrosion current. B) A rotating magnetic field generated by the rotation of the magnetized shafting parts, including the ship's magnetic propeller and the main shaft [9]. It can be verified that the latter part is related to the rotation speed of the propeller with a frequency is around hertz. The rotating propeller can be considered as a rotating magnetic dipole when the detection distance is much longer than the propeller length [10].

In this paper, the magnetic field generated by the rotating magnetic propeller is modeled, and an inversion-based calculation is utilized to present a location mechanism for the magnetic source with only one magnetic sensor when the magnetic moment is known. In section II, the ship shaft-rate magnetic field is modeled. In section III, the magnetic location algorithm is proposed. In section IV, the rotating magnetic dipole's magnetic field is simulated, and the location algorithm accuracy is analyzed. In section V, the experiments are performed to verify the location algorithm. Finally, the conclusion and future research directions are provided in section VI.

II. MODELING OF THE SHIP SHAFT-RATE MAGNETIC FIELD

A ship propeller is a magnetic object. When the magnetic field is detected in the air, the detection distance is much longer than the propeller length. Thus, the rotating propeller can be considered as a rotating magnetic dipole [11]. Consider that the propeller shaft is along the z-axis, and the xyz space coordinate system is established. The magnetic dipole moment is located at the $D\,(x_0, y_0, z_0)$ and rotates around the z-axis at with frequency f; the observation point is located at the coordinate origin, the dipole magnetic moment is denoted by $\vec{m}$ with the magnitude M. The magnetic moment component of $\vec{m}$ on the z axis is denoted by $\vec{m}_z$, the magnetic moment component on the xy plane is indicated by $\vec{m}_{xy}$, and the angular velocity of the magnetic moment $\vec{m}_{xy}$ on the xy plane is denoted by ω, $\omega = 2\pi f$. The equivalent diagram is shown in Fig. 1.

Consider that the magnetic moment components of the magnetic dipole $\vec{m}$ in the x-axis, y axis and z- axis directions are denoted by $m_p m_f$ and m_l, respectively. Now the following relations can be written:

$$\begin{cases} m_p = m_{xy} cos\,(\omega t + \alpha_0) \\ m_f = m_{xy} sin\,(\omega t + \alpha_0) \\ m_l = m_z \end{cases} \tag{1}$$

where α_0 is the initial angle between the $\vec{m}_{xy}$ and the x-axis. According to (1), we observed that the magnetic moment of a rotating magnetic dipole [12] can be decomposed into $m_p m_f$ and m_l. According to Biot-Savart law, the magnetic induction intensity of a dipole with magnetic moment $\vec{m}$ at distance $\vec{r}$

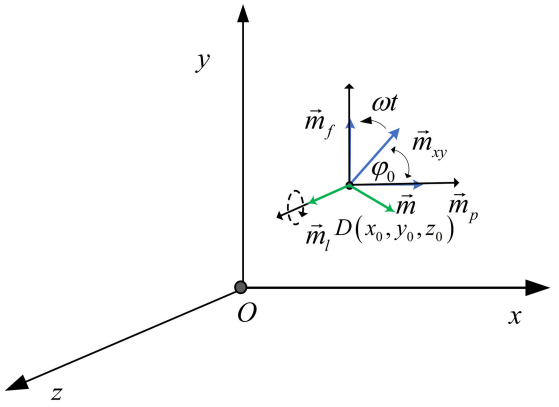

FIGURE 1. The coordinate system of the rotating magnetic dipole.

can be calculated as [13]:

$$\vec{B} = \frac{\mu_0}{4\pi r^3}[\frac{3(\vec{m}\cdot\vec{r})\cdot\vec{r}}{r^2} - \vec{m}] \tag{2}$$

And μ_0 is the magnetic permeability ($\mu_0 = 4\pi \times 10^{-7}$), $r = \sqrt{x_0^2 + y_0^2 + z_0^2}$.

Consider that the magnetic induction intensities generated by the magnetic moments $m_p m_f$ and m_l are denoted by $\vec{B}_p$, $\vec{B}_f$ and $\vec{B}_l$, respectively. Now, the three components of $\vec{B}_p$, $\vec{B}_f$ and $\vec{B}_l$ can be obtained as:

$$\vec{B}_p = (B_{px}, B_{py}, B_{pz}), \begin{cases} B_{px} = \dfrac{\mu_0 m_p}{4\pi}\left(\dfrac{3x_0^2}{r_1^5} - \dfrac{1}{r_1^3}\right) \\ B_{py} = \dfrac{\mu_0 m_p}{4\pi}\cdot\dfrac{3x_0 y_0}{r_1^5} \\ B_{pz} = \dfrac{\mu_0 m_p}{4\pi}\cdot\dfrac{3x_0 z_0}{r_1^5} \end{cases}$$

$$\vec{B}_f = (B_{fx}, B_{fy}, B_{fz}), \begin{cases} B_{fx} = \dfrac{\mu_0 m_f}{4\pi}\cdot\dfrac{3x_0 y_0}{r_1^5} \\ B_{fy} = \dfrac{\mu_0 m_f}{4\pi}\left(\dfrac{3y_0^2}{r_1^5} - \dfrac{1}{r_1^3}\right) \\ B_{fz} = \dfrac{\mu_0 m_f}{4\pi}\cdot\dfrac{3y_0 z_0}{r_1^5} \end{cases}$$

$$\vec{B}_l = (B_{lx}, B_{ly}, B_{lz}), \begin{cases} B_{fx} = \dfrac{\mu_0 m_l}{4\pi}\cdot\dfrac{3x_0 z_0}{r_1^5} \\ B_{fy} = \dfrac{\mu_0 m_l}{4\pi}\cdot\dfrac{3y_0 z_0}{r_1^5} \\ B_{fz} = \dfrac{\mu_0 m_l}{4\pi}\cdot\left(\dfrac{3z_0^2}{r_1^5} - \dfrac{1}{r_1^3}\right) \end{cases} \tag{3}$$

According to formula (2) and (3), we have:

$$\begin{aligned} \vec{B} &= \left(B_x, B_y, B_z\right) = \vec{B}_p + \vec{B}_f + \vec{B}_l \\ &= \left(B_{px} + B_{fx} + B_{lx}, B_{py} + B_{fy} + B_{ly}, B_{pz} + B_{fz} + B_{lz}\right) \end{aligned} \tag{4}$$

III. THE MAGNETIC LOCALIZATION ALGORITHM

The relations between the observed magnetic field and the point coordinates are derived to obtain the target coordinates.

A. THE CALCULATION OF EIGENVECTOR $\vec{B}_{pf}$

According to the vector relations and the induced magnetic field direction, we can calculate the eigenvectors of the vectors $\vec{B}_p$ and $\vec{B}_f$. Consider that the eigenvector is denoted by $\vec{B}_{pf}$. It can be obtained as:

$$\vec{B}_{pf} = \vec{B}_p \times \vec{B}_f \tag{5}$$

Now, the three components of $\vec{B}_{pf}$ can be obtained as:

$$\begin{aligned} B_{pfx} &= B_{py} \cdot B_{fz} - B_{pz} \cdot B_{fy} \\ B_{pfy} &= B_{px} \cdot B_{fz} - B_{pz} \cdot B_{fx} \\ B_{pfz} &= B_{px} \cdot B_{fy} - B_{py} \cdot B_{fx} \end{aligned} \tag{6}$$

According to relations (1), (3) and (4), the properties of $\vec{B}_p$ and $\vec{B}_f$ can be analyzed. It can be observed that the magnetic induction intensities $\vec{B}_p$ and $\vec{B}_f$ can be calculated when the magnetic induction intensity $\vec{B}$ is multiplied by cosine and sine variables $cos\,(\omega \cdot t)$ and $sin\,(\omega \cdot t)$, respectively, and integrated. Accordingly, the following relation can be obtained:

$$\begin{cases} B_{\mathrm{px}} = \dfrac{2\int_0^T B_x \cdot cos\,(\omega \cdot t)\,dt}{T} cos\,(\omega t + \alpha_0) \\ B_{\mathrm{py}} = \dfrac{2\int_0^T B_y \cdot cos\,(\omega \cdot t)dt}{T} cos\,(\omega t + \alpha_0) \\ B_{\mathrm{pz}} = \dfrac{2\int_0^T B_z \cdot cos\,(\omega \cdot t)dt}{T} cos\,(\omega t + \alpha_0) \end{cases}$$
$$\begin{cases} B_{\mathrm{fx}} = \dfrac{-2\int_0^T B_x \cdot sin\,(\omega \cdot t)dt}{T} sin\,(\omega t + \alpha_0) \\ B_{\mathrm{fy}} = \dfrac{-2\int_0^T B_y \cdot sin\,(\omega \cdot t)\,dt}{T} sin\,(\omega t + \alpha_0) \\ B_{\mathrm{fz}} = \dfrac{-2\int_0^T B_z \cdot sin\,(\omega \cdot t)\,dt}{T} sin\,(\omega t + \alpha_0) \end{cases} \tag{7}$$

Assuming:

$$\begin{cases} b_1 = \dfrac{2\int_0^T B_x \cdot cos\,(\omega \cdot t)\,dt}{T} & b_2 = \dfrac{-2\int_0^T B_x \cdot sin\,(\omega \cdot t)dt}{T} \\ b_3 = \dfrac{2\int_0^T B_y \cdot cos\,(\omega \cdot t)dt}{T} & b_4 = \dfrac{-2\int_0^T B_y \cdot sin\,(\omega \cdot t)\,dt}{T} \\ b_5 = \dfrac{2\int_0^T B_z \cdot cos\,(\omega \cdot t)dt}{T} & b_6 = \dfrac{-2\int_0^T B_z \cdot sin\,(\omega \cdot t)\,dt}{T} \end{cases} \tag{8}$$

So we can get:

$$\begin{aligned} \frac{B_{pfx}}{B_{pfy}} &= \frac{b_3 b_6 - b_5 b_4}{-b_1 b_6 + b_5 b_2} \\ \frac{B_{pfy}}{B_{pfz}} &= \frac{-b_1 b_6 + b_5 b_2}{b_1 b_4 - b_3 b_2} \end{aligned} \tag{9}$$

For easy observation, assume:

$$\begin{aligned} c_1 &= b_3 b_6 - b_5 b_4 \\ c_2 &= -b_1 b_6 + b_5 b_2 \\ c_3 &= b_1 b_4 - b_3 b_2 \end{aligned} \tag{10}$$

For the B_x, B_y and B_z are the measured magnetic field, the eigenvector $\vec{B}_{pf}\left[B_{pfx}, B_{pfy}, B_{pfz}\right]$ can be obtained from (7). Then, c_1, c_2, and c_3 can be calculated by using (8), (10).

B. CALCULATION OF THE MAGNETIC DIPOLE'S COORDINATES

According to the relations (3) and (6), the three components of eigenvector $\vec{B}_{pf}$ can be calculated as:

$$\begin{aligned} B_{pfx} &= \frac{\mu_0^2 M_p M_f}{(4\pi)^2}\left(\frac{3x_0y_0}{r_0^5} \times \frac{3y_0z_0}{r_0^5} - \frac{3x_0z_0}{r_0^5}\left(\frac{3y_0^2}{r_0^5} - \frac{1}{r_0^3}\right)\right) \\ B_{pfy} &= \frac{\mu_0^2 M_p M_f}{(4\pi)^2}\left(\left(\frac{1}{r_0^3} - \frac{3x_0^2}{r_0^5}\right)\frac{3y_0z_0}{r_0^5} + \frac{3x_0z_0}{r_0^5} \times \frac{3x_0y_0}{r_0^5}\right) \\ B_{pfz} &= \frac{\mu_0^2 M_p M_f}{(4\pi)^2}\left(\left(\frac{3x_0^2}{r_0^5} - \frac{1}{r_0^3}\right)\left(\frac{3y_0^2}{r_0^5} - \frac{1}{r_0^3}\right) - \frac{3x_0y_0}{r_0^5}\right. \\ &\quad \left. \times \frac{3x_0y_0}{r_0^5}\right) \end{aligned} \tag{11}$$

where r_0 is the distance between the observed point and the magnetic dipole. By simplifying 11, we have:

$$\begin{aligned} B_{pfx} &= \frac{3x_0z_0\mu_0^2 M_p M_f}{16\pi^2 r_0^8} \\ B_{pfy} &= \frac{3y_0z_0\mu_0^2 M_p M_f}{16\pi^2 r_0^8} \\ B_{pfz} &= \frac{\mu_0^2 M_p M_f\left(-3\left(x_0^2 + y_0^2\right) + r_0^2\right)}{16\pi^2 r_0^8} \end{aligned} \tag{12}$$

From formula (12), we can get:

$$\begin{aligned} \frac{B_{pfx}}{B_{pfy}} &= \frac{c_1}{c_2} = \frac{x_0}{y_0} \\ \frac{B_{pfy}}{B_{pfz}} &= \frac{c_2}{c_3} = \frac{3y_0z_0}{-3\left(x_0^2 + y_0^2\right) + r_0^2} = \frac{3y_0z_0}{-2r_0^2 + 3z_0^2} \end{aligned} \tag{13}$$

Now, the relationship between the eigenvector $\vec{B}_{pf}$ and the coordinates of the magnetic source can be obtained from (13).

Besides, it can be seen that the magnetic field at the observation point is elliptically polarized from relation (1) of the rotating magnetic dipole. Thus the minimum magnetic induction intensity B_{min} at the observation point and the distance r_0 between it and the magnetic dipole should satisfy the following relations:

$$B_{min} = min\left(\sqrt{B_x^2 + B_y^2 + B_z^2}\right) = \frac{\mu_0 M}{4\pi r_0^3} \tag{14}$$

$$x_0^2 + y_0^2 + z_0^2 = r_0^2 \tag{15}$$

When the magnetic induction intensity $\left(B_x, B_y, B_z\right)$ of the observation point is measured, the three components c_1, c_2 and c_3 can be calculated. Relations (13-15), and the target range can be utilized to calculate the position coordinates (x_0, y_0, z_0).

IV. SIMULATION RESULTS

This simulation is performed to verify the localization algorithm feasibility and evaluate the proposed method accuracy.

A. THE SIMULATION OF THE MAGNETIC FIELD OF THE ROTATING MAGNETIC DIPOLE

In this section, the positioning simulation of the rotating magnetic dipole is performed to evaluate the proposed algorithm. Consider the magnetic moment of the rotating magnetic dipole as $m_l = 100A \cdot m^2, m_{xy} = 1000A \cdot m^2$, $M = \sqrt{m_l^2 + m_{xy}^2}$, the rotation frequency $f = 5\text{Hz}$, where $\omega = 2\pi f$. Suppose that the magnetic source coordinates are chosen as $D\,(30, 20, 25)$, and the distance between it and the measured point is denoted by r, Thus, $r = \sqrt{x_0^2 + y_0^2 + z_0^2} = 43.875m$.

The magnetic induction intensity of the rotating dipole at the measured point $O\,(0, 0, 0)$ versus time is shown in Fig. 2.

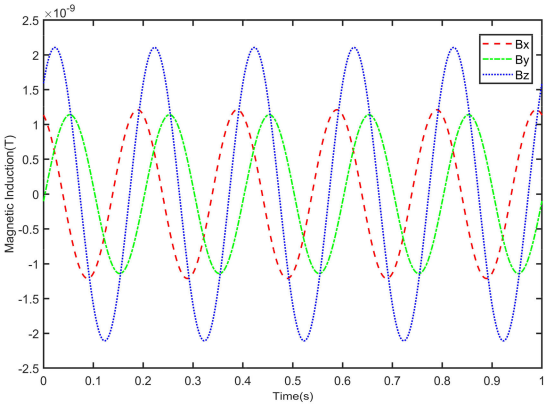

FIGURE 2. The time domain diagram of the magnetic induction intensity at point *O*.

It was stated that α_0 is the initial angle between the magnetic moment $\vec{m}_{xy}$ and the x-axis. Now, by considering $\alpha_0 = \left[0, \frac{\pi}{3}, \frac{2\pi}{3}, \pi, \frac{4\pi}{3}, \frac{5\pi}{3}\right]$, take angle integer of $\frac{\pi}{3}$ corresponding to different initial angles. Then, the values of B_{px}, B_{py}, B_{pz}, B_{fx}, B_{fy}, and B_{fz} can be obtained at six different initial angles. The obtained values are shown in Fig. 3.

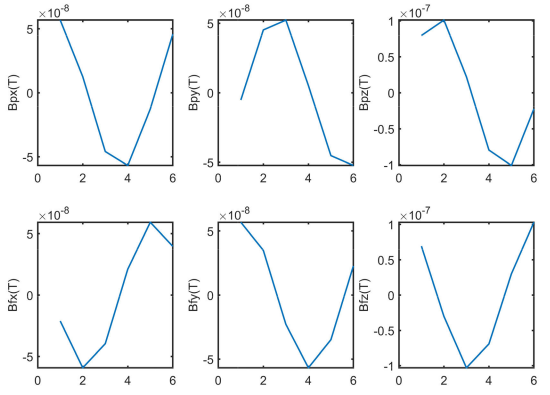

FIGURE 3. The magnetic components of $\vec{B}_p$ and $\vec{B}_f$ at six different initial angles.

The values of c_1, c_2 and c_3 for six different initial angles of the rotating magnetic field can be obtained through relations (8) and (10). The obtained simulations are shown in Fig. 4.

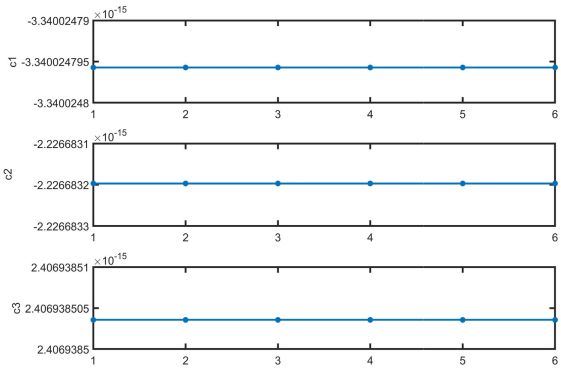

FIGURE 4. The values of c_1,c_2 and c_3 at different initial angles.

As shown in Fig. 4, the values of the c_1, c_2 and c_3 are independent of the initial angle. That means that c_1, c_2 and c_3 will not be affected by the initial angle. In the actual location, the data in any period of the observed magnetic field can be utilized for location calculation.

B. THE LOCATION ACCURACY ANALYSIS

The magnetic dipole is chosen as $x_0 = 5, y_0 = 3$, and its z coordinate is selected every 1 meter from the $z = 0.5m$ for a total of 50 measuring points. The observed point is at $O\,(0, 0, 0)$. The magnetic moment of the rotating magnetic dipole is considered as $m_l = 100A \cdot m^2, m_{xy} = 1000A \cdot m^2$, According to the location algorithm in Section 3, the magnetic source coordinates can be obtained from the three components of the magnetic field at the measuring point. The calculated the theoretical values of the location method are presented in Fig. 5.

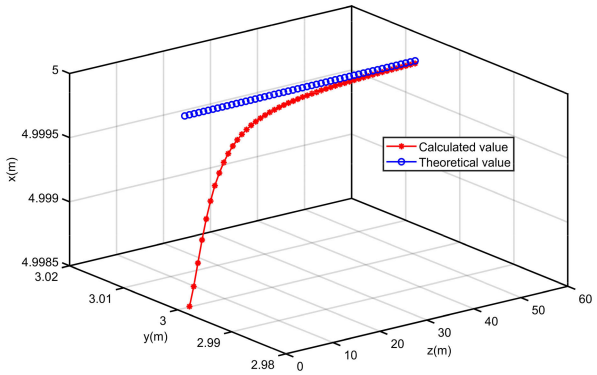

FIGURE 5. The calculated and theoretical values of positioning coordinate points.

As shown in Fig. 5, as the z coordinate increases, the calculated value gradually tends to the theoretical one. In the location simulation, the absolute errors between the calculated values and theoretical ones for the three-axis coordinate of the observation point are shown in Fig. 6, while the relative errors of three-axis are shown in Fig. 7.

According to Fig. 6 and Fig. 7, as the z coordinate increases, the absolute errors of x and y axes decrease,

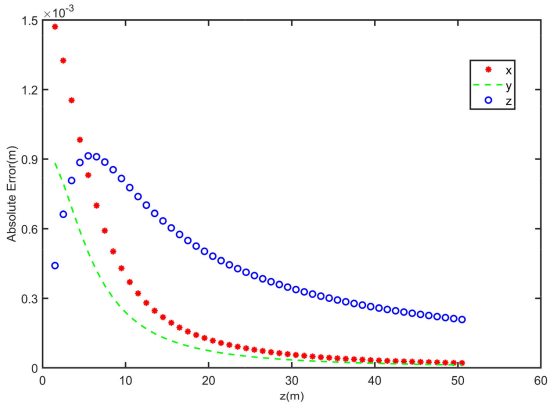

FIGURE 6. The absolute errors of the triaxial coordinate.

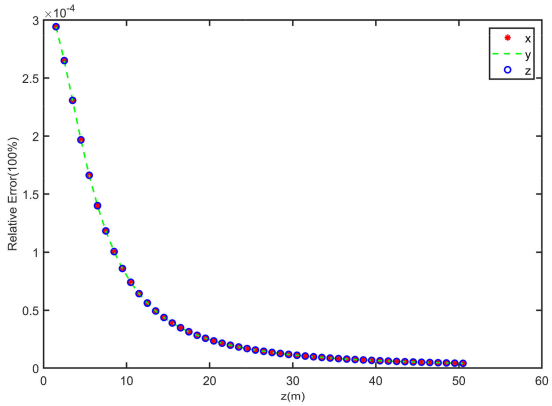

FIGURE 7. The relative errors of the triaxial coordinate.

while the absolute errors of the z-axis first increase and then decrease, and the relative errors of the triaxial coordinate gradually decrease, with a maximum of 0.03%. The reason is that the absolute error of z-axis is related to the values of x-axis and y-axis. However, the maximum absolute error of all axes is only 0.0015m. It can be concluded that the location algorithm has high accuracy and can meet the location requirements.

C. THE MEASUREMENT NOISE INFLUENCE ON THE LOCATION ACCURACY

The magnetic field of the rotating dipole is a kind of sinusoidal signal with a specific frequency. The measurement noise is generally a stochastic signal. In the experiment process, the measurement noise can be significantly eliminated by filtering. Therefore, it is relatively small, mainly includes the instrument noise. If the measurement noise is about 0.1nT, the simulation conditions are similar to the corresponding ones in section B. The magnetic source coordinate is taken every 1 meter along with the z = 0.5m, while 50 points are considered. Now, the absolute and relative errors of the three-axis coordinate are shown in Fig. 8 and Fig. 9, respectively.

According to Fig. 8 and Fig. 9, when 0.1nt measurement noise is added, the absolute and relative errors increase with the increase of the z-axis coordinate. When the z-axis coordinate is less than 30, the relative and absolute errors of

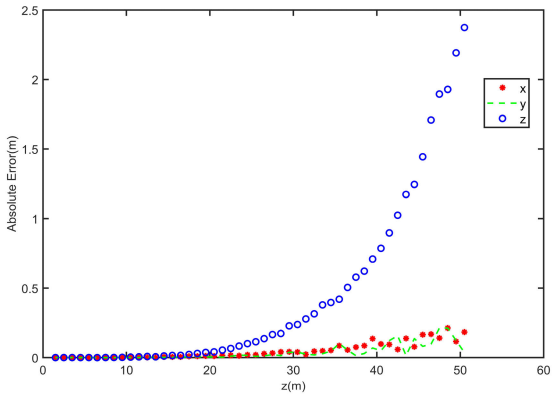

FIGURE 8. The absolute errors of triaxial coordinates with 0.1nT measurement noise.

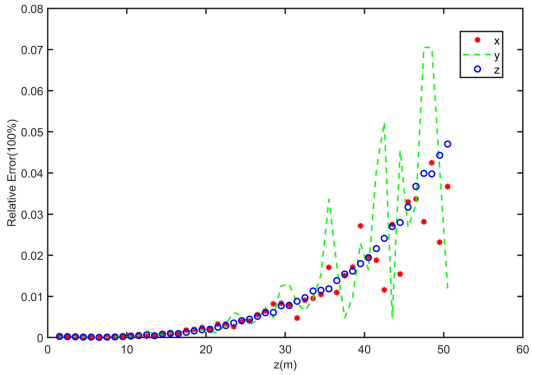

FIGURE 9. The relative errors of triaxial coordinates with 0.1nT measurement noise.

triaxial coordinates increase slowly, while the absolute error is less than 0.25m, and the relative error is less than 1.3%. When the z-axis distance exceeds 30m, absolute and relative errors begin to increase rapidly. The reason is that when the measurement distance is increased, the rotating magnetic field intensity decreases, which strengthens the influence of the measurement noise on the rotating magnetic field, and leads to a higher positioning error. It can be seen that the measurement distance is confined by the measurement noise and the rotating magnetic intensity, and the application distance of the positioning algorithm can be reduced with the noise. In this simulation experiment with the measurement noise, the measurement distance is about 30m.

V. EXPERIMENTAL RESULTS

In this experiment, the site is selected on an extensive playground near a small forest with a relatively stable magnetic environment. A cylindrical magnet made of Nd-Fe-B is utilized to simulate a rotating propeller and generate a rotating magnetic field with the magnetic moment $M = 3Am^2$. The center of the Nd-Fe-B magnet is considered as the magnetic source point to establish a coordinate system. The three-axis fluxgate developed by our research group independently is employed to measure the rotating magnetic field at 80 points. The 80 points are selected at eight directions, while 10 points are chosen at 1m interval in each direction. The acquisition card's sampling frequency is 400Hz, while the rotating

frequency of Nd-Fe-B magnetic is 2.5Hz. Fig. 10 shows the schematic of the rotating Nd-Fe-B magnetic. Fig. 11 shows the test measurement scenario.

FIGURE 10. The schematic of rotating Nd-Fe-B magnetic.

FIGURE 11. The test measurement scenario.

First, a point O (5, 3, 0.1) is randomly chosen to verify the rotating magnetic field distribution. Now, the distribution of the three components of the measured magnetic field B_x , B_y,B_z and the total magnetic field B_{total} are presented in Fig. 12.

The interferences of static magnetic field, power frequency magnetic field, and harmonic waves, such as geomagnetic field and trend term, are eliminated to obtain the rotating magnetic field. The distribution is shown in Fig. 13.

The spectrogram of the rotating magnetic field is shown in Fig. 14.

Fig. 13 demonstrates the compatibility of the rotating magnetic field signal with the simulation model diagram. At the same time, as shown in Fig. 14, the filtered signal frequency is mainly concentrated in the low-frequency range. It can be observed that the maximum spectrum value can be found at 2.5hz, which is compatible with the rotating frequency of

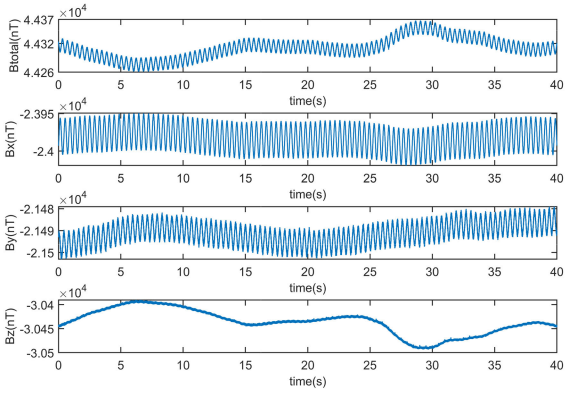

FIGURE 12. The triaxial components of the measured and total magnetic fields.

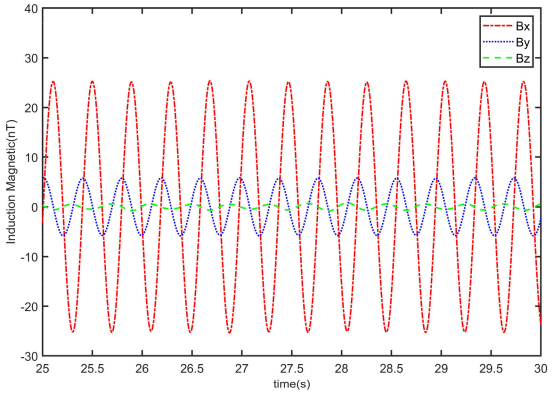

FIGURE 13. The triaxial components of the rotating magnetic field.

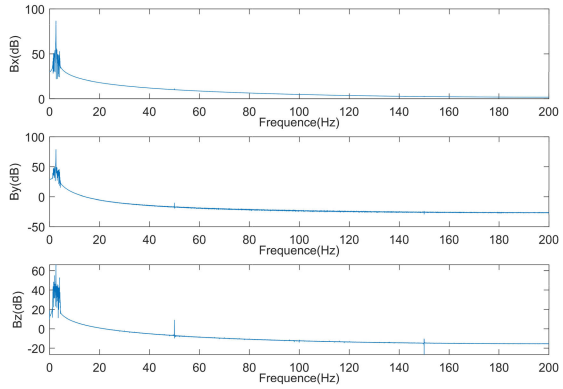

FIGURE 14. The spectrogram of the rotating magnetic field.

TABLE 1. The absolute and relative errors of the triaxial coordinate.

	Absolute error (m)	Relative error (100%)
Maximum	0.45	7.4%
Minimum	0.03	1.2%
Mean	0.26	3.7%

the Nd-Fe-B magnet. The positioning results of 80 points are presented in Table 1.

Table 1 shows that the mean relative error is 3.7%, demonstrating the accuracy of the location method. The maximum

relative error is about 7.4%. The experimental errors are higher than the simulation ones. The main reason is that the measurement distance of some points is relatively short, which significantly influences the equivalent rotating dipole. Besides, the positioning error may be due to the measurement error of the distance and the experimental equipment sensitivity.

VI. CONCLUSION

In this paper, the rotating propeller is considered as a rotating magnetic dipole. The magnetic source can be located only by the measured magnetic induction intensity (B_x, B_y, B_z) at one measuring point under the predefined value of the magnetic moment of the magnetic source. The rotating magnetic dipole location algorithm can be utilized to detect and locate the underwater rotating magnetic field. Finally, the experiments are performed to evaluate the feasibility of the rotating magnetic model. However, due to the experiment limitations like the measurement distance, measurement error, and experimental equipment sensitivity, the obtained value for the actual positioning error is higher than the theoretical error. Besides, when the measurement distance increases, the location algorithm will no longer be accurate due to the weak signal and the noise influence. As a further study, an appropriate algorithm should be combined with the positioning algorithm to detect the mentioned weak signal.

ACKNOWLEDGMENT

The authors thank Chunsheng Lin for offering considerable help which has improved the work and thank him for patiently answering some questions about rotating magnetic dipole.

REFERENCES

[1] J. T. Weaver, "The quasi-static field of an electric dipole embedded in a two-layer conducting half-space," *Can. J. Phys.*, vol. 45, no. 6, pp. 1981–2002, Jun. 1967, doi: 10.1139/p67-156.
[2] R. Adey and J. Baynham, "Predicting corrosion related electrical and magnetic fields using BEM," in *Proc. Undersea Defence Technol. Eur.*, London, U.K., 2000, p. 473.
[3] W. Jia and C. Lin, "Improved Euler method for preventing failure of positioning magnetic target magnetic Gradiometer," *J. Navigat. Univ. Eng.*, vol. 30, no. 03, pp. 37–42, 2018.
[4] G. Yin, L. Zhang, H. Jiang, Z. Wei, and Y. Xie, "A closed-form formula for magnetic dipole localization by measurement of its magnetic field vector and magnetic gradient tensor," *J. Magn. Magn. Mater.*, vol. 499, Apr. 2020, Art. no. 166274, doi: 10.1016/j.jmmm.2019.166274.
[5] S. Song, X. Qiu, J. Wang, and M. Q.-H. Meng, "Design and optimization strategy of sensor array layout for magnetic localization system," *IEEE Sensors J.*, vol. 17, no. 6, pp. 1849–1857, Mar. 2017, doi: 10.1109/JSEN.2017.2652470.
[6] W. Jia and C. Lin, "Research on magnetic target location method based on a single magnetic gradiometer," *Acta Armamentarii*, vol. 38, no. 8, pp. 1572–1577, 2017.
[7] S. A. Fares, R. Fleming, D. Dinn, and C. J. Purcell, "Horizontal and vertical electric dipoles in a two-layer conducting medium," *IEEE Trans. Antennas Propag.*, vol. 62, no. 11, pp. 5656–5665, Nov. 2014, doi: 10.1109/tap.2014.2355295.
[8] Y. Sui, K. Leslie, and D. Clark, "Multiple-order magnetic gradient tensors for localization of a magnetic dipole," *IEEE Magn. Lett.*, vol. 8, May 2017, Art. no. 6506605, doi: 10.1109/LMAG.2017.2708682.
[9] G. Yin, L. Zhang, H. Jiang, Z. Wei, and Y. Xie, "A closed-form formula for magnetic dipole localization by measurement of its magnetic field vector and magnetic gradient tensor," *J. Magn. Magn. Mater.*, vol. 499, Apr. 2020, Art. no. 166274, doi: 10.1016/j.jmmm.2019.166274.
[10] Z. Sun, L. Maréchal, and S. Foong, "Passive magnetic-based localization for precise untethered medical instrument tracking," *Comput. Methods Programs Biomed.*, vol. 156, pp. 151–161, Mar. 2018, doi: 10.1016/j.cmpb.2017.12.018.
[11] J. Liu, X. Li, and X. Zeng, "A real-time magnetic dipole localization method based on cube magnetometer array," *IEEE Trans. Magn.*, vol. 55, no. 8, pp. 1–9, Aug. 2019, doi: 10.1109/TMAG.2019.2910481.
[12] F. Kuckes and N. Y. Ithaca, "Rotating magnet for distance and direction measurements from a first borehole to a second borehole," U.S. Patent 5 589 775, Dec. 31, 1996.
[13] T. Nara, H. Watanabe, and W. Ito, "Properties of the linear equations derived from Euler's equation and its application to magnetic dipole localization," *IEEE Trans. Magn.*, vol. 48, no. 11, pp. 4444–4447, Nov. 2012, doi: 10.1109/TMAG.2012.2196418.

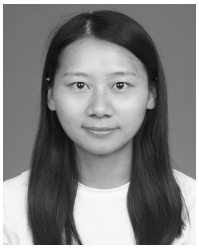

PENGFEI LIN was born in Dongying, Shandong, China, in 1991. She received the B.S. degree in communication engineering from the China University of Petroleum (East China), in 2014, and the M.S. degree in circuit system from the Naval University of Engineering, Wuhan, China, in 2016, where she is currently pursuing the Ph.D. degree. Her research interests include target's magnetic field study and magnetic source detection and location.

NING ZHANG was born in 1981. He received the Ph.D. degree from the Naval University of Engineering, Wuhan, China, in 2011. He is currently an Associate Professor with the Naval University of Engineering. His research interests include target's magnetic field study, aeromagnetic detection, and magnetic compensation.

MING CHANG was born in Kaifeng, Henan, China, in 1986. He received the B.S. and M.S. degrees from the Naval University of Engineering, where he is currently pursuing the Ph.D. degree. His research interests include target magnetic field characteristics, signal processing, and magnetic source tracking.

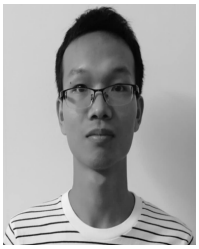

LEI XU was born in Zaoyang, Hubei, China, in 1993. He received the B.S. degree in performance test and fault diagnosis from the Ordnance Engineering College, in 2016, and the M.S. degree in performance test and fault diagnosis from Army Engineering University, Shijiazhuang, in 2018. He is currently pursuing the Ph.D. degree with the Naval University of Engineering. His research interests include magnetic field study of target and magnetic source detection and location.